Using Multispectral Remote Sensing to Track Evapotranspiration Patterns in the Yinchuan Plain

Junzhen Meng , Xiaoquan Yang , Zhiping Li * , Guizhang Zhao , Peipei He , Yabing Xuan , Yunfei Wang

Posted Date: 8 August 2024

doi: 10.20944/preprints202408.0555.v1

Keywords: Evapotranspiration; geeSEBAL; Land use types; Landsat remote sensing data

Article

Using Multispectral Remote Sensing to Track Evapotranspiration Patterns in the Yinchuan Plain

Junzhen Meng [1], Xiaoquan Yang [1], Zhiping Li [2,*], Guizhang Zhao [1], Peipei He [1], Yabing Xuan [1] and Yunfei Wang [1]

[1] North China University of Water Resources and Electric Power, Zhengzhou 450046, China
[2] Henan Vocational College of Water Conservancy and Environment, Zhengzhou 450046, China
* Correspondence: lizhiping@ncwu.edu.cn

Abstract: Evapotranspiration is a critical component of the hydrological cycle, and it has a decisive impact on the ecosystem balance in arid and semi-arid regions. The Yinchuan Plain, located in the Gobi of Northwest China, has a strong surface ET. In order to assess the ET pattern in this region, we obtained the actual ET(ET_a) of Yinchuan Plain between 1987 and 2020 using the GEE platform. Specifically, we used the Landsat TM+/OLI remote sensing imagery and GEE Surface Energy Balance Model (geeSEBAL) to analyze the change pattern of ET over different seasons, years, and land types. The results show that: (1) the daily ET_a of the Yinchuan Plain is the highest in the central lake wetland area in spring, with a maximum value of 4.32 mm day^{-1}; In summer, it is concentrated around the croplands and water bodies, with a maximum value of 6.90 mm day^{-1}; In Autumn and winter, it is mainly concentrated around the water bodies and impervious areas, with maximum values of 3.93 and 1.56 mm day^{-1}, respectively. (2) From 1987 to 2020, the ET of the Yinchuan Plain showed an obvious upward and downward trend in some areas with significant land use changes, but the overall ET of the region remained relatively stable without dramatic fluctuations. (3) The ranking ET_a values for different land use types in the Yinchuan Plain region is as follows: water body>cultivated land>impervious>grassland>bare land. Our results showed that geeSEBAL is highly applicable in the Yinchuan Plain area. It allows for the accurate and detailed inversion of ET in the study area, which facilitates the study of regional hydrological cycle and water governance.

Keywords: evapotranspiration; geeSEBAL; Land use types; Landsat remote sensing data

1. Introduction

Evapotranspiration (ET) plays an important role in the hydrological cycle and energy exchange in ecosystems such as the biosphere and the atmosphere[1]. Studies have shown that 70% of the precipitation on the earth's surface is returned to the atmosphere through ET[2]. Especially in agricultural ecosystems of arid and semi-arid zones, ET is an important factor in maintaining water and energy balance. In these areas, the evaporative losses account for more than 80% of the total water consumption[3]. The surface heat and water balance has a major influence on geographic transformations, and a clear understanding of ET is important for the better understanding of the energy balance and water cycle over large scales. Remote sensing has been used to estimate surface ET since the 1970s with the purpose of efficiently monitoring and quantifying water exchange processes[4,5]. Obtaining spatial and subsurface parameters, vegetation and soil information from remote sensing can effectively help measure daily ET at the surface[6–9]. Models for estimating ET based on remote sensing can be mainly classified into three categories: statistical empirical methods, energy residual methods, and full remote sensing model.

Statistical empirical methods are easily affected by vegetation cover and weather conditions[10,11], and the full remote sensing model can achieve good inversion results in some arid areas. However, the inversion of ET in croplands or forest needs to be further researched and validation[12]. Residual method of the energy balance is used to invert the net radiative flux, soil heat

 doi:10.20944/preprints202408.0555.v1

flux and sensible heat flux by remote sensing technology to calculate the latent heat flux residual according to the surface energy balance equation, so as to derive the surface ET[13]. The residual method can be generally categorized into two types: single layer models and double layer models. Single layer models needn't distinguish the ET exchanges between soil and vegetation, and are commonly used to estimate surface ET, which is strongly influenced by land surface temperature (Ts). Widely used single layer models include SEBI (Surface Energy Balance Index)[14], SEBAL (Surface Energy Balance Algorithm for Land)[15–19], SEBS (Surface Energy Balance System)[20–22], and Simplified Surface Energy Balance (SSEBop)[23]. These models have different sensitivities to Ts and meteorological inputs. The SSEBop requires high quality hourly and daily meteorological data inputs[24–26], which has a large impact on the applicability of ET estimation, especially in areas lacking ground meteorological data. On the other hand, SEBAL has a lower sensitivity to the meteorological data input and a higher sensitivity to Ts [27,28], which greatly improves the model's applicability and lowers the threshold for the ET estimation with the remote sensing model. The double layer models proposed by Shuttleworth[29–31] in 1988, not only consider the energy exchange at the surface, but also incorporate vegetation characteristics and soil heat conduction. The double layer model is not extensively utilized because its impedance calculations employ empirical methods, making them more sophisticated and vulnerable to geo-graphical limitations.

The Yinchuan Plain area is an important agricultural hub in the Yellow River Basin, but it lacks high precision long-term meteorological data. Moreover, there exists few cases of applying remote sensing methods in inverting ET using high resolution data series. Meanwhile, due to the complexity of traditional remote sensing methods, surface ET inversions have been conducted in 5-to-10-year intervals and without spatial and temporal continuity. To compensate for this issue, we utilized a new tool namely geeSEBAL developed based on the GEE platform and SEBAL for the estimation of surface ET, using Landsat5(TM+) and Landsat8(OLI) remote sensing images. The state-of-the-art meteorological reanalysis ERA5-Land data has been used to obtain the multi-year actual evapotranspiration (ET_a) in the Yinchuan Plain area from 1987 to 2020. The main objective has been to analyze the ET change pattern of the Yinchuan Plain area over different seasons, years and land types.

2. Materials and Methods

2.1. Study Area

The Yinchuan Plain is situated in the central part of the Ningxia Hui Autonomous Region, flanked by the Yellow River on both sides. Bounded by the Ordos Plateau to the east, the Helan Mountains to the west, the Loess Plateau to the south and Shizuishan to the north, the study area lies between approximately 37°29′ to 38°53′ N and 105°49′ to 106°53′ E(Figure 1.). Although the plain is situated in a temperate arid zone, the annual average precipitation reaches merely 200 mm. The annual water discharge of the Yellow River passing through the region reaches an average of $300\times10^8 m^3$, making it an important industrial and agricultural hub in the middle and upper reaches of the Yellow River, and an important core area of the national economic development of Ningxia Hui Autonomous Region and surrounding areas. The annual evaporation of the Yinchuan Plain is as high as 1600mm, which has a significant impact on the ecology of the Yinchuan Plain. This area relies heavily on the river runoff supply, which can become an important restricting factor the development of local industries and agriculture[32].

 doi:10.20944/preprints202408.0555.v1

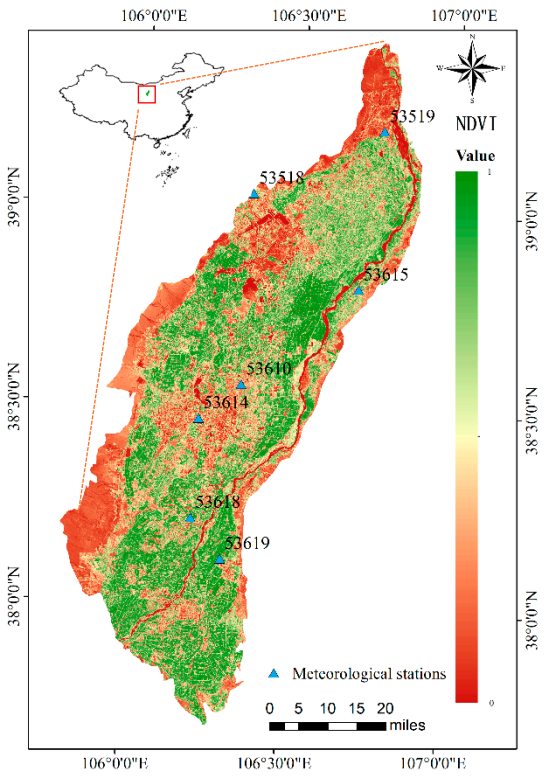

Figure 1. The Yinchuan Plain Area.

2.2. Data Sources

Since the Yinchuan Plain covers a wide area of 7790 km², it requires high quality remote sensing images. In this study, some 40 high quality Landsat5(TM+) and Landsat8(OLI) images between 1989 and 2020 were selected to cover the whole study area. These images were employed to estimate ET_a from the surface parameters (Table 1.). The ERA5 Land Reanalysis dataset was used as the meteorological data input for the geeSEBAL [33,34]. This dataset contains hourly data on air temperature at 2 m, dew point temperature, and eastward and northward wind speed at 10 m. Relative humidity estimation follows Shuttleworth[35], and more detailed information on data input can be found in[36].

The meteorological data were collected from Ningxia Meteorological Bureau, and used to estimate the reference ET based on the FAO-Penman-Monteith method[37]. Due to the lack of flux tower observations, the large and small ET data from meteorological stations were used as geeSEBAL ET validation data. The large evaporation pan was made of a 60cm wide fiberglass plastic drum buried in the ground, and the evapotranspiration was close to the surface ET_a. Small evaporator (20cm in diameter) was made from galvanized iron or other alloys. In dry areas or dry seasons, the outer wall of the pan has higher temperatures given its small size which makes the observed values significantly larger than the real water surface evaporation. Therefore, the obtained values cannot accurately represent the real condition of free water surface evaporation. Likewise, estimating and tracking the actual land surface evaporation from these values become challenging, but it has certain reference value for understanding the changes and trends of water surface evaporation over time[38]. More detail about the evaporator used can be found in Specification for Surface Meteorological Observations[39].

The China Land Cover Dataset (CLCD), used to calculate ET for different sub-surfaces, is provided by Xin Huang from Wuhan University[40], who produced the annual CLCD based on 335,709 Landsat images from Google Earth Engine. This dataset contains annual land cover information of China from 1990-2020. The author has elicited spatiotemporal features based on all available Landsat data on GEE using the Random Forest Classifier. The author has also proposed a post-processing method including spatiotemporal filtering and logical inference to further improve

 doi:10.20944/preprints202408.0555.v1

the consistency of the CLCD. Finally, the overall accuracy of CLCD reaches 80% based on 5,463 visual decoding samples, meeting the accuracy requirements for this experiment.

Table 1. Remote sensing images and end member criterion.

Remote Sensing Image	$NDVI_{cold}$	Ts_{cold}	$NDVI_{hot}$	Ts_{hot}
LT05_129033_19870920	5%	20%	10%	20%
LT05_129033_19890824	5%	20%	10%	20%
LT05_129033_19910830	5%	20%	10%	1%
LT05_129033_19920816	5%	20%	10%	20%
LT05_129033_19930616	5%	20%	10%	20%
LT05_129033_19940822	5%	20%	10%	20%
LT05_129033_19960811	5%	20%	10%	1%
LT05_129033_19990820	5%	20%	10%	1%
LT05_129033_20010809	5%	20%	10%	1%
LT05_129033_20020625	5%	20%	10%	1%
LT05_129033_20060908	5%	20%	10%	1%
LT05_129033_20070709	5%	10%	1%	10%
LC08_129033_20180824	5%	10%	1%	10%
LC08_129033_20200813	5%	10%	1%	10%

2.3. Methods

2.3.1. The geeSEBAL Algorithm

SEBAL is a commonly used large-scale remote sensing ET assessment model that uses the energy of longwave and shortwave radiations from the sun and the atmosphere to estimate soil and surface layers heating and ET. It divides the net surface radiative fluxes into three components: soil heat flux, sensible heat flux, and latent heat flux. The energy balance equation is:

$$\lambda E = R_n - H - G \quad (1)$$

where λE is the latent heat flux (W/m²), R_n is the surface net radiation flux (W/m²) (Eq. 2), H is the sensible heat flux (W/m²) and G is the soil heat flux (W/m²)(Eq 3).

Net surface radiation (netradiation) is the main source of energy for the process of heat flux transfer and exchange in surface water. Soil heat flux is the state of heat exchange between the surface and deeper soil layers .

$$R_n = (1-\alpha)R_S\downarrow + R_L\downarrow - R_L\uparrow - (1-\varepsilon_0)R_L\downarrow \quad (2)$$

$$\frac{G}{R_n} = \alpha(T_s - 273.15)(0.0038\alpha + 0.0074\alpha^2)(1 - 0.98NDVI^4) \quad (3)$$

where α is the surface albedo, caculated according to Tasumi and Ke[32,41], T_s is the surface temperature, $R_S\downarrow$ is the incoming shortwave radiation, $R_L\downarrow$ is the incoming longwave radiation, $R_L\uparrow$ is the outgoing longwave radiation, and ε_0 is the surface thermal emissivity.

Daily ET is computed by upscaling instantaneous λE to ET_a($\wedge$ is the intermediate variable)(Eq 4).

$$\mathrm{ETa}_{24\mathrm{h}} = \frac{\wedge R_{n24h}}{\lambda} \quad (4)$$

Where $\mathrm{ETa}_{24\mathrm{h}}$ is the daily ET (mm); R_{n24h} is the daily average net radiation (W/m2); $\wedge$ is the evaporative fraction; λ is the latent heat of water evaporation (J/Kg).

Evaporative fraction $\wedge$ is the intermediate variable.

 doi:10.20944/preprints202408.0555.v1

$$\Lambda = \frac{\lambda E}{R_n - G} \quad (5)$$

Where Λ is the evaporative fraction; λE is the latent heat flux (W/m²); R_n is the net radiation (w/m²); G is the soil heat flux (w/m²).

The SEBAL algorithm used in this paper was implemented in the GEE platform using the JavaScrip language[36]. The GEE platform provides well-established Landsat datasets and meteorological data such as ERA5. The ERA5 is the fifth generation of the ECMWF (European Centre for Medium-Range Weather Forecasts) atmospheric reanalysis dataset of the global climate from January 1950 until now. This dataset provides hourly estimates of a large number of atmospheric, terrestrial and oceanic climate variables, which allows geeSEBAL to handle ET on global to regional scales, especially in areas where ground meteorological data is limited. The geeSEBAL provides long term and comprehensive reference ET values, The operation process of this program can be found in the references [36].

It is worth noting that the specific humidity in geeSEBAL is not archived directly in ERA dataset. The archive contains near-surface (2m from the surface) temperature, dew point temperature, and surface pressure from which one can calculate specific humidity at 2m. The specific humidity at 2 meter q_{sat} were calculated according to Eq 6-7 (for more info refer to [42]) . In these equations the dew point temperature T and surface pressure p (which is approximately equal to the pressure at 2m) are approximated at the height of 2m.

$$q_{\text{sat}} = \frac{\frac{R_{\text{dry}}}{R_{\text{vap}}} e_{\text{sat}}(T)}{p - \left(1 - \frac{R_{\text{dry}}}{R_{\text{vap}}}\right) e_{\text{sat}}(T)} \quad (6)$$

where the R_{dry} and R_{vap} are gas constants for dry air and water vapor. The constants are defined in [42]. The saturation vapor pressure is expressed with the Teten's formula:

$$e_{sat}(T) = a_1 \, exp\left\{a_2 \left(\frac{T - T_0}{T - a_3}\right)\right\} \quad (7)$$

with the parameters set according to Buck (1981)[43] for saturation over water (a_1 = 611.21 Pa, a_2 = 17.502 and a_3 = 32.19 K) and to the AERKi formula of Alduchov and Eskridge[44] for saturation over ice (a_1 = 611.21 Pa, a_2 = 22.587 and a_3 = −0.7 K), with T_0 = 273.16 K.

2.3.2. Hot and Cold Endmembers: Automated Calibration

There are two important assumptions in the SEBAL model: (i) there is a linear relationship between the geothermal temperature difference dT, and the surface temperature Ts(Eq 8.); (ii) there are both cold and hot image elements in the study area, with the H of the cold and hot image elements being 0 and (Rn - G), respectively.

$$dT = a + b \cdot T_s \quad (8)$$

where a and b are the empirical regression coefficients.

The first assumption serves to simplify the problem of solving the linear coefficients of the surface radiant temperature Ts; the second assumption, which introduces two cases of ET extremes (0 for the cold image element H, 0 for the hot image element LE), will thus solve for the coefficients of the linear relationship described above, and thus for H over the entire region.

The geeSEBAL supports simplified automated statistical algorithm to select the hot and cold endmembers, which is based on the version of the Calibration using Inverse Modeling at Extreme Conditions (CIMEC) algorithm used in METRIC[45]. The NDVI and T are usually used as the cold and hot endmember candidates, for example in a semi-arid climate. Here the cold endmember is selected within a set of candidates with the highest NDVI (5%), and the lowest Ts (20%) percentiles. Conversely, the hot endmember is selected based on the lowest NDVI (10%) and the highest Ts (20%) percentiles[45]. In this study, we performed the selection of hot and cold end members based on the NDVI and T of each image according to the thresholds provided in Table 1.

2.3.3. Statistical Analysis

RMSD(Root Mean Square Deviation) and the Bias value were used to evaluate the consistency between ET estimated by geSEBAL and ET measured by meteorological stations (Eq 9-10). R^2 is used

 doi:10.20944/preprints202408.0555.v1

as the correlation analysis between ET_a and potential evapotranspiration by PM model to comprehensively evaluate the applicability of geeSEBAL in the Yinchuan Plain.

$$\mathrm{RMSE} = \sqrt{\sum_{i=1}^{n} \frac{(Y_i - \bar{Y}_i)^2}{n}} \quad (9)$$

$$Bias = \sum_{i=0}^{n} \frac{(Y_i - \bar{Y}_i)}{n} \quad (10)$$

2.3.4. Mann-Kendall Trend Analysis

Mann-Kendall(MK) nonparametric test was used in this study to reveal the trend of ET changes in the Yinchuan Plain area. The MK method has no requirement on the distribution of the sample data, which works well for not normally distributed hydrological data[46]. The MK method defines the statistic S as Eq 11:

$$S = \sum_{j=1}^{n-1} \sum_{k=j+1}^{n} s(Y_k - Y_j) \quad (11)$$

where the Y1, Y2,… , Yn are the time series variables and n is the length of the time series.

$$s(Y_k - Y_j) = \begin{cases} +1, Y_k > Y_j \\ 0, Y_k = Y_j \\ -1, Y_k < Y_j \end{cases} \quad (12)$$

Where Y_j and Y_k are the corresponding measurements for the years j and k, respectively, and k>j.

$$Z = \begin{cases} \frac{S-1}{\sqrt{V(S)}}, S > 0 \\ 0, S = 0 \\ \frac{S+1}{\sqrt{V(S)}}, S < 0 \end{cases} \quad (13)$$

Where Z is a normally distributed statistic and V(S) is the variance. At a given α confidence level, $Z > 0$ indicates an upward trend and $Z < 0$ indicates a downward trend. The statistics $|Z| \geq 1.96$ and $|Z| \geq 2.58$ mean significance at 95% and 99% confidence levels, respectively.

3. Results

3.1. geeSEBAL ET Validation

Four meteorological sites with longer time-series and large ET values were selected for validation (2000-2020) (Figure 2.). Meanwhile, to ensure the accuracy of the longtime ET series, meteorological stations with relatively complete and small ET values from 1990-2010 were selected as geeSABAL validation sites (Figure 3.).

The comparison of geeSEBAL ET and the observed values (Figure 2.) showed moderate-to-high accuracy in Yinchuan plain area. The average Bias was estimated -0.11 mm day^{-1} close to 0, ranging from -0.87 mm day^{-1} to 0.80 mm day^{-1}. The average RMSD was measured 1.12 mm day^{-1} without a clear bias pattern, ranging from 0.83 to 1.47 mm day^{-1}, which demonstrates a wide range of applicability.

The comparison of geeSEBAL with large evapotranspiration values at some of the meteorological stations showed lower R^2 values, such as both meteorological stations 53615 and 53519 which are distributed along the Yellow River. Station 53615 had the highest RMSD and Bias as 1.47 mm day^{-1} and -0.87 mm day^{-1} respectively, and the lowest R^2 as 0.12 mainly due to two reasons. On the one hand, the Landsat remote sensing were scarce in dry seasons. On the other hand, the limited number of years with actual large ET values, resulted in large time spans between the data. Although R^2 was not as high as expected in four meteorological stations in large ET comparison, the R^2 showed higher correlation for most of the stations in samll ET values, reaching up to 0.82 (Figure 3.). As for stations 53614 and 53615, there was a good consistency between large and small ETs. Although weak correlation was detected between the geeSEBAL and observed ET values, the estimated values were still within a reasonable range with RMSD of 1.47 mm day^{-1} .

 doi:10.20944/preprints202408.0555.v1

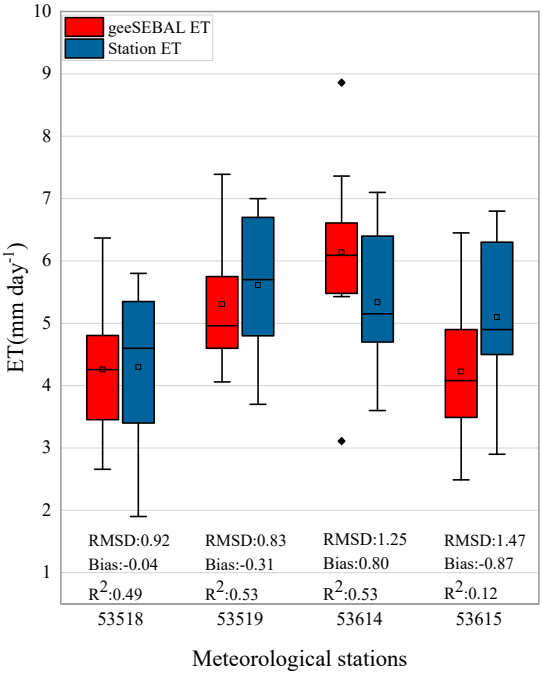

Figure 2. Comparison between meteorological stations with large ET and geeSEBAL ET. Diamond shaped points represent outliers lying outside the 150% inter-quartile range.

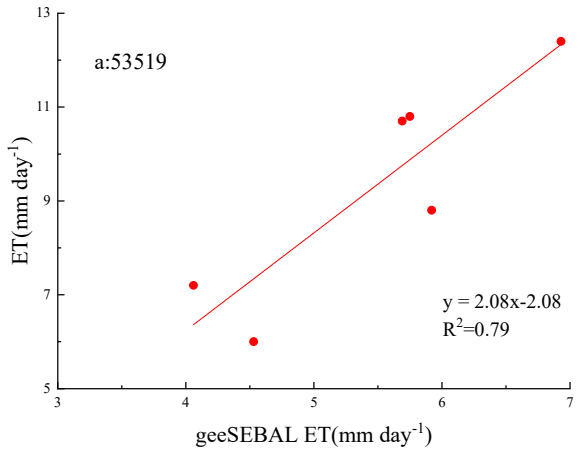

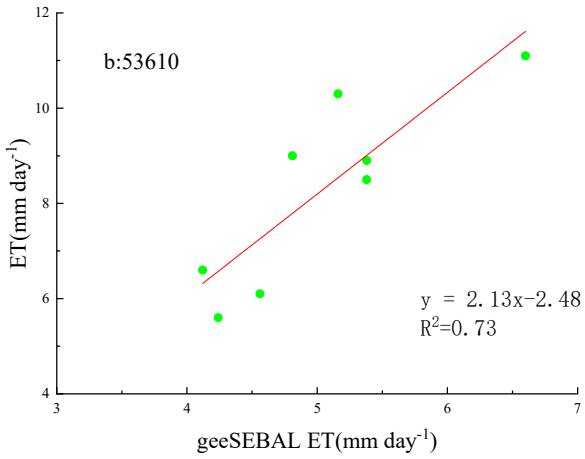

 doi:10.20944/preprints202408.0555.v1

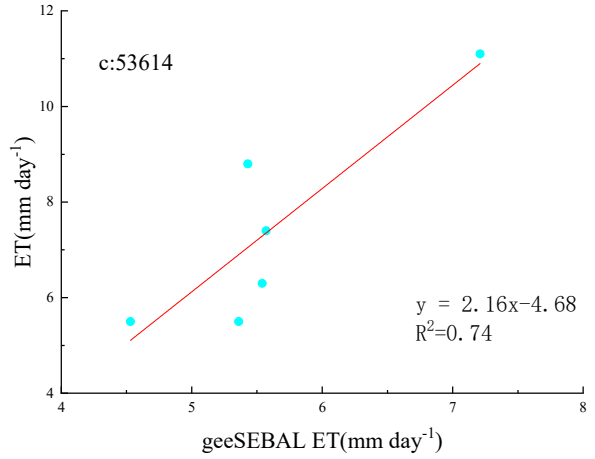

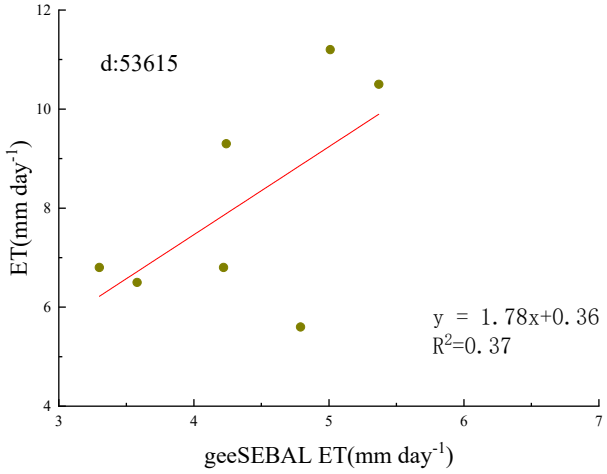

 doi:10.20944/preprints202408.0555.v1

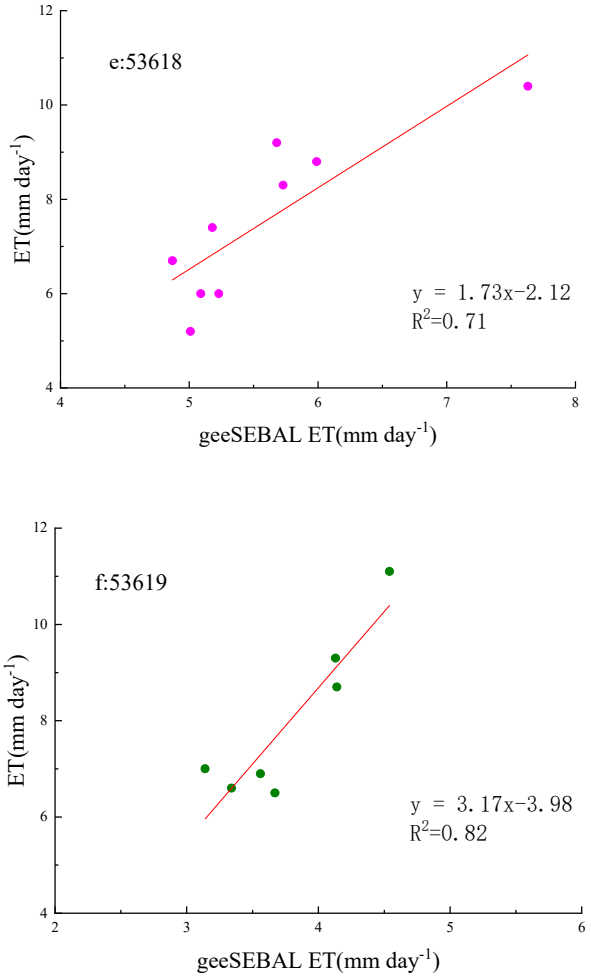

Figure 3. Comparison between observed ET values and geeSEBAL ET.

Table A5 Land reanalysis using the optimized percentiles and the standard percentiles recommended by Allen et al[45]. The model sensitivity to meteorological factors affects ET inversion results. Due to the large span of Yinchuan Plain and the complex geomorphology, the surface ET results of remote sensing inversion are uncertain. This paper analyzes the inversion results from the geSEBAL and PM based on quantitative aspects. The surface ET obtained by inversion based on the geeSEBAL model was analyzed in correlation with the values obtained from the potential ET(ET_P) calculated by the P-M model (Figure 4.). Only in site 53619, a weak correlation with R^2 of 0.43 was detected. The rest of the stations showed strong correlations with R^2 ranging from 0.62 to 0.79. In summary, the surface ET inversion accuracy in the Yinchuan Plain using the geSEBAL model was relatively high indicating that the model has high applicability in arid and semi-arid areas.

 doi:10.20944/preprints202408.0555.v1

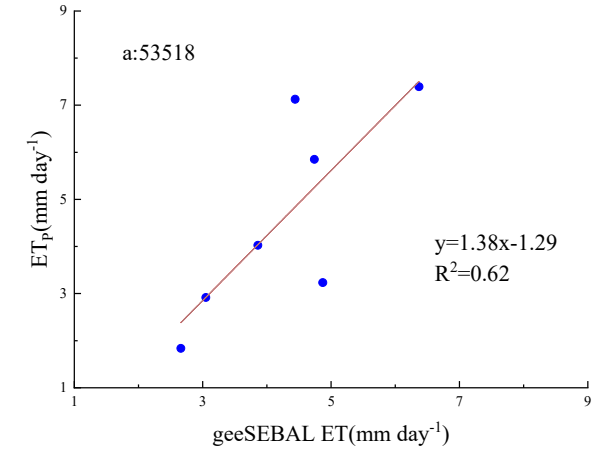

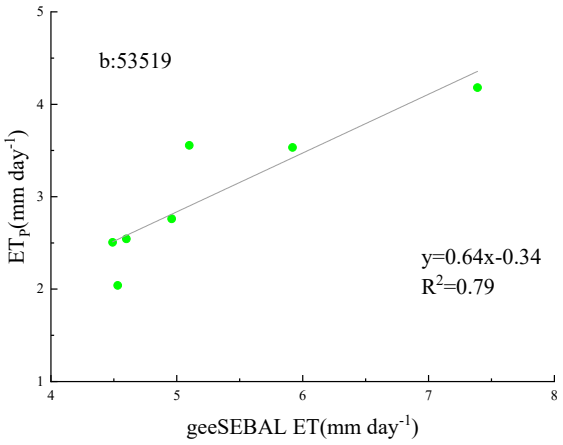

 doi:10.20944/preprints202408.0555.v1

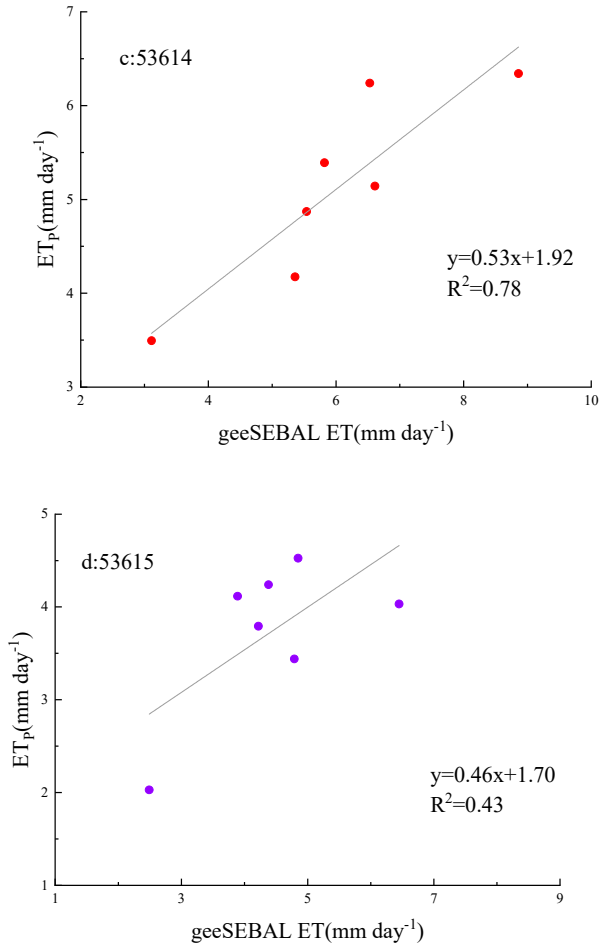

Figure 4. Comparison between ET_P and geeSEBAL ET.

3.2. Changing Patterns of Evapotranspiration in Yinchuan Plain

3.2.1. Changing Trend of ET

Table 2 shows the dates of the images in four seasons in the Yinchuan Plain. From the spatial distribution of spring ET in Figure 5(a), it can be seen that the northern and southern regions have lower ET values in the range of 0-3 mm day^{-1}. The ET is greater on water bodies and around the Yinchuan City, with a maximum value of 4.32 mm day^{-1}. It is mainly due to the existence of broad lakes and wetlands around Yinchuan City which is known as the "International Wetland City". There are five national wetland parks around this City, with the Yinchuan Plain wetland covering more than 80% of the total area and acting as the main source of spring ET in this region .

Figure 5(b) shows the spatial distribution of ET in the Yinchuan Plain in summer. The ET values from bare land and impervious areas are relatively lower ranging between 0-4 mm day^{-1}. The main reason for lower ET values is owing to the presence of impervious areas. From the ET spatial distribution it can be seen that water bodies and arable lands are the main sources of ET in summer, with the highest value of 6.90 mm day^{-1}.

Figure 5(c) shows that the ET in the fall is more uniformly distributed. In this case, water bodies have the highest ET of 3.93 mm day^{-1}. Leaving crop lands fallow has resulted in lower ET values in the range of 1-3 mm day^{-1}. Figure 5(d) shows that the highest ET of 1.56 mm day^{-1} occurred in winter. Although this result is affected by the quality of the image, but it can be seen that ET in water bodies and impervious areas is generally higher than that of cultivated land and bare land.

 doi:10.20944/preprints202408.0555.v1

Table 2. Seasonal images and end member criterion.

Season	Image Data	$NDVI_{cold}$	Ts_{cold}	$NDVI_{hot}$	Ts_{hot}
Spring	LC08_129034_20200306	5%	20%	10%	10%
Summer	LC08_129033_20200813	5%	20%	10%	20%
Autum	LC08_129033_20201016	5%	20%	10%	20%
Winter	LC08_129033_20140117	5%	10%	1%	10%

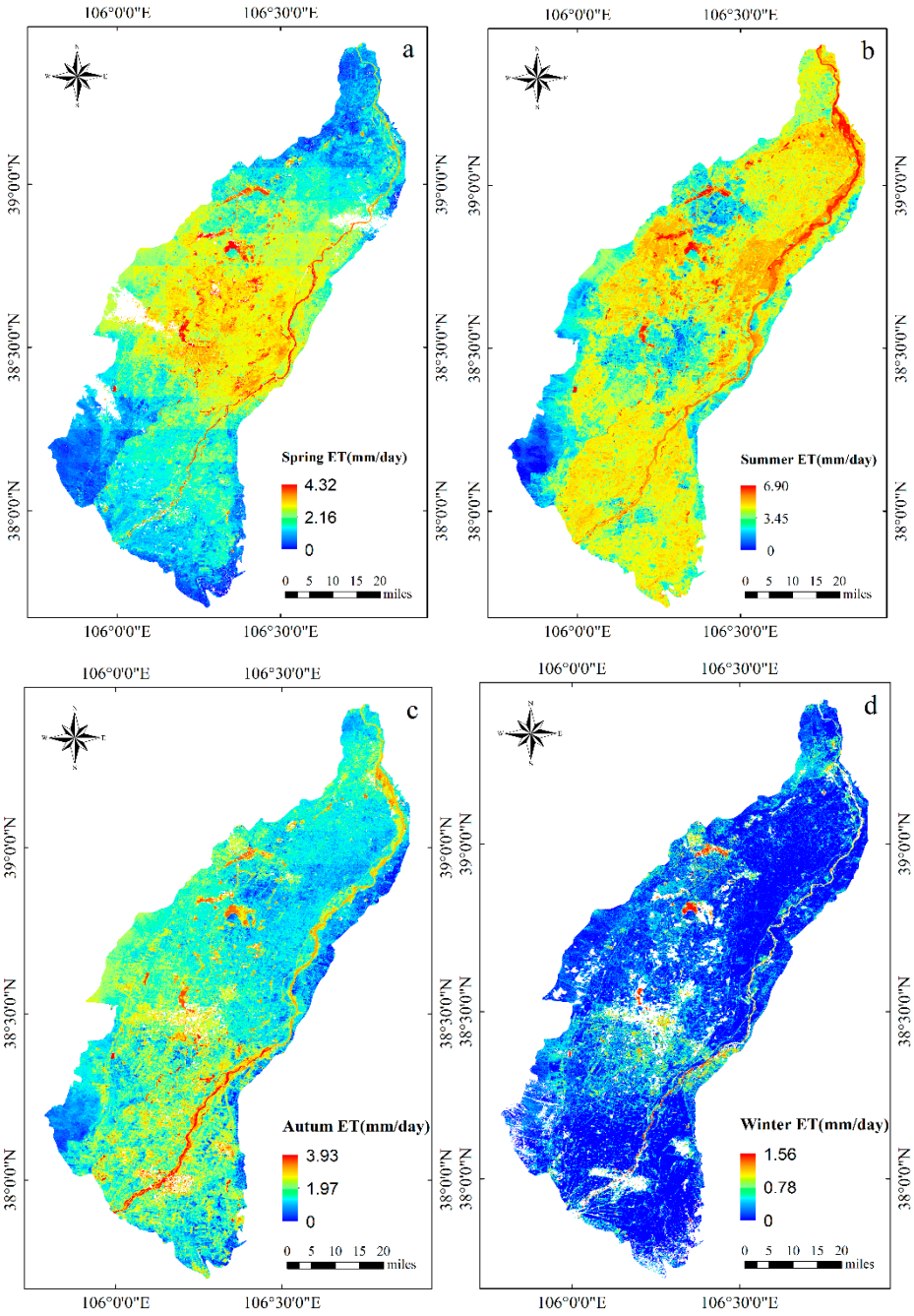

Figure 5. Seasonal ETa changes in the Yinchuan Plain.

To obtain long-term ET trends in the Yinchuan Plain area, a total of 22 representative images were selected. These images, acquired from June to August between 1989 and 2020, offer a complete coverage of the study area (Table 1.). Surface ET trend was obtained using MK trend analysis (Figure 6.).

 doi:10.20944/preprints202408.0555.v1

The overall ET changes in the Yinchuan Plain are mostly concentrated in the western section, impervious areas and along the Yellow River, with confidence intervals exceeding 99%. ET changes in the vegetated areas (arable land and grassland) are not obvious, and the majority of the confidence intervals are lower than 95%. The ET in the western region and some areas along the Yellow River showed an increasing trend However, in several major residential areas (Shizuishan City, Yinchuan City, Wuzhong City) it showed a decreasing trend. Our results showed that the areas with significant ET alterations have undergone considerable land-use changes. Land use changes from bare lands to croplands, wetlands and water bodies resulted in a decreasing ET trend. At the same time, land use conversion from cropland to impervious areas resulted in an increasing ET trend. The trend of ET reflects the land use changes to a certain extent. In order to further explore the distribution pattern of ET in the Yinchuan Plain, the contribution of different land uses to ET values is discussed in detail in chapter 3.2.2.

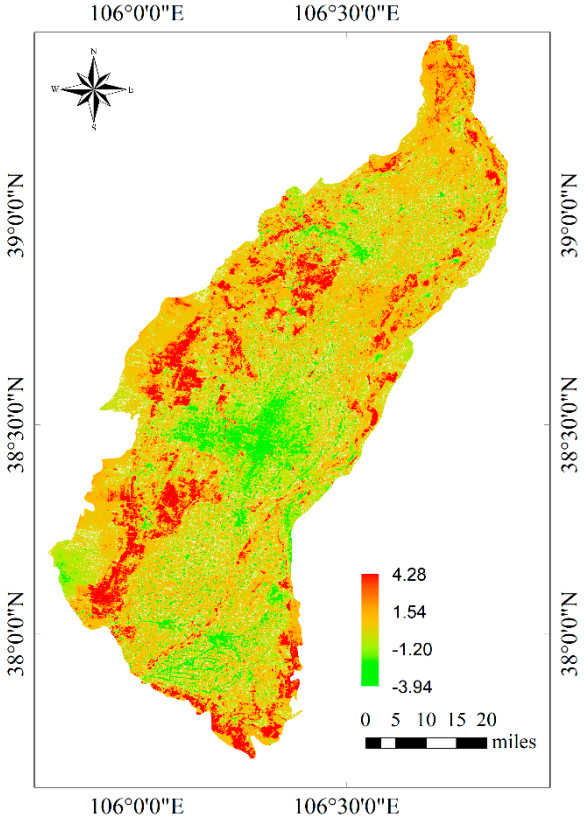

Figure 6. Trends of ET_a in the Yinchuan Plain in 1987-2020.

3.2.2. Contribution of Soil Evaporation and Transpiration to ET Change

The variation of evapotranspiration (ET) is influenced by meteorology, vegetation cover type, and other factors. Additionally, there are significant disparities in the physical and chemical properties of different land use types in the subsurface. These disparities result in diverse responses of the surface to solar radiation. Furthermore, there can be substantial differences in surface radiation and energy distribution within similar subsurface areas, leading to a non-uniform distribution of ET across the land surface. In order to investigate the ET_a changes of different sub-surfaces in the Yinchuan Plain, land surface ET from 1990 to 2020 was used along with the CLCD land use dataset. The land use types in the Yinchuan Plain could be grouped into five main categories: cropland, grassland, water body, bare land, impervious land (Figure 7.).

 doi:10.20944/preprints202408.0555.v1

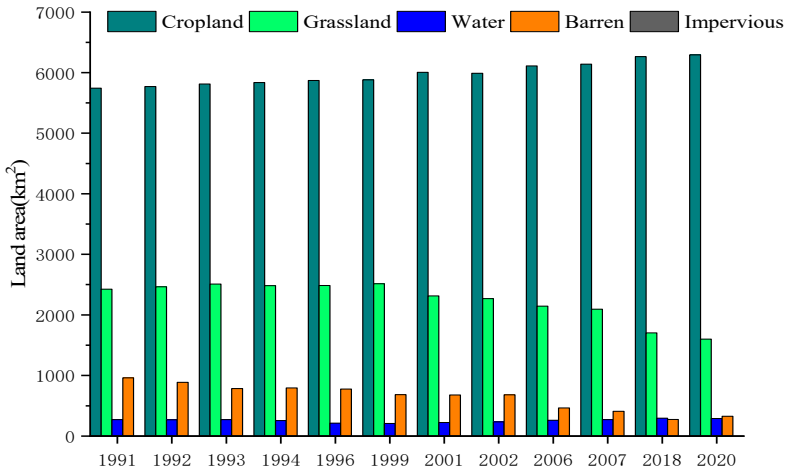

Figure 7. Area of Yinchuan Plain land use types.

As shown in Figure 8, the daily ET of different land use types is in the following order: water bodies > cropland > impervious > grassland > bare land. The ET of different types showed obvious stratified characteristics and highly consistent trends. The fluctuation amplitude of each line reflects the response of different subsurface types to climatic factors. Among them, the ET of water body fluctuates between 5.03-7.62 mm day^{-1}, as the most sensitive to the influence of meteorological factors, such as temperature, wind speed, and surface radiation, etc. Cultivated land and grassland, as the main land use types in Yinchuan Plain, show opposite trends with the ET of cultivated land ranging 4.16-6.36 mm day^{-1}, and ET of grassland ranging 2.07- 3.78 mm day^{-1}. This is mainly due to low transpiration in grasslands. In the Yinchuan Plain, rice paddy is the main agricultural land use type where water is more abundant during the growing season in summer. Increased sunlight hours lead to increased evapotranspiration (ET) values, which are twice as large as those in grasslands. Bare lands and impervious areas are the two land use types with large rate of changes in the Yinchuan Plain. Conversion of bare lands into built-up and impervious areas has altered ET in this region. In this manner, the amount of ET in the impervious areas ranges 3.28-5.27 mm day^{-1}, while it ranges 0.81-2.67 mm day^{-1} in the bare lands.

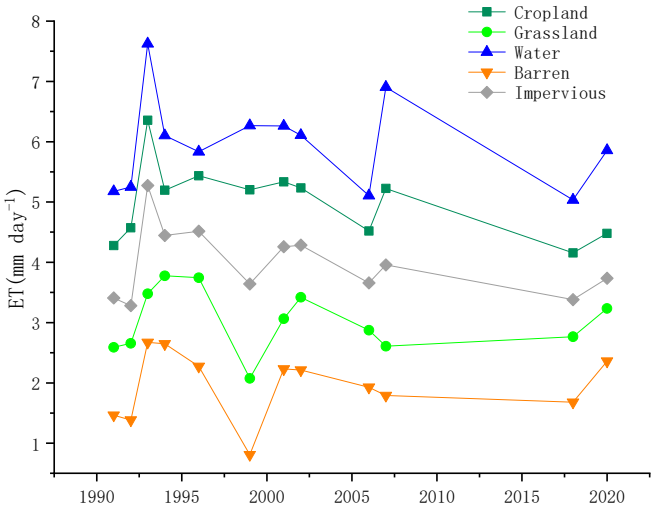

Figure 8. ET_a in different subsurface types.

Human activities often have significant impacts on natural systems and may even determine the evolution of regional microclimates and ecosystems in arid and semi-arid regions. For example, human activities have dominated the evolution of hydro-ecological processes in the lower Tarim

 doi:10.20944/preprints202408.0555.v1

River for centuries[47]. The most apparent manifestation of human activities in the Yinchuan Plain region could be regarded as land use conversion. In order to more intuitively respond to the distribution pattern of ET in the Yinchuan Plain and under different land use types, the contribution of ET(σ) of different types (Figure 9.) was calculated as in Eq. 14.

$$\sigma_C = \frac{ET_C}{ET_C+ET_G+ET_W+ET_B+ET_I} \quad (14)$$

Where the σ_C is the contribution ET of cropland, and ET_C-ET_I is the evaportranpiration of different land use types.

Before 1996, the σ was in the order of Cropland>Grassland>Bareland>Water body>Impervious. After 1996, the order changed into Cropland>Grassland>Impervious>Water body>Bare land. Among the different vegetated land use types, croplands contributed between 68% and 78% to the total ET, followed by grassland contributing between 13% and 21%. Areas with sparse vegetation including water bodies, bare lands and impervious areas accounted for less than 10% of the total ET. In summary, croplands are the main source of evapotranspiration in the Yinchuan Plain. This implies that the impact of human activities has become one of the most important factors dominating evapotranspiration in the region. The primary focal points for hydrological cycle conservation and water governance in the future appear to be cropland and vegetation management.

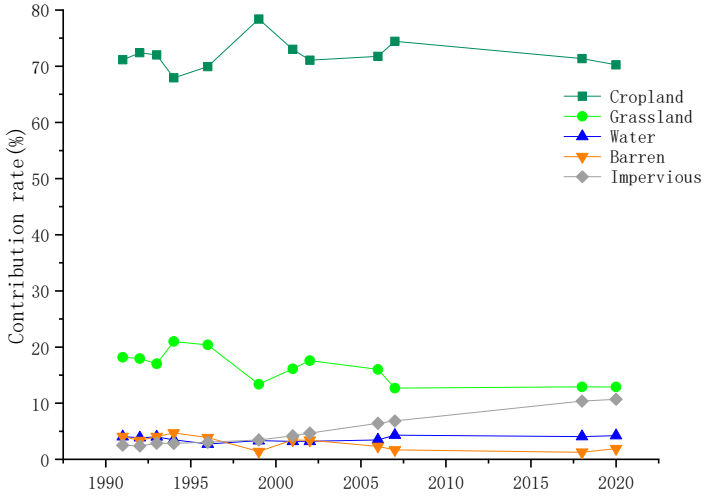

Figure 9. ET_a contribution of different subsurface types.

4. Discussion

4.1. The Effects on ET Trends

In this paper, the spatiotemporal variation pattern of evapotranspiration in the Yinchuan Plain from 1987 to 2020 was studied from two aspects: one is the distribution of ET in different seasons, and the other is the trend of ET changes in long-term series. Comparing the summer ET distribution in Figure 5(b) with the summer variation trend in Figure 8, the maximum difference in ET variation among different land types can reach 5.46 mm day^{-1}, while the maximum difference in ET variation among the same land type is only 2.59 mm day^{-1}. This indicates that the variation of surface ET is greatly influenced by different underlying surfaces, and that human activities are one of the important factors affecting regional ET variation. Studies have shown that meteorological factors such as temperature and rainfall also have an important impact on ET. Xiaomei Jin et al[48] analyzed the impact of monthly average temperature and rainfall on ET in the Yinchuan Plain using actual data, and found an R^2 of 0.82 between ET and temperature, while it was only 0.38 between ET and rainfall. At the same time, meteorological factors such as sunshine hours, wind speed, and relative humidity also affect surface evapotranspiration to varying degrees[49,50]. For example, Wang et al[51] found that a decrease in local sunshine hours in Yangtze River basin would reduce the energy source of surface evapotranspiration, thereby weakening the process of surface evapotranspiration.

 doi:10.20944/preprints202408.0555.v1

In summary, it can be seen that the factors affecting surface ET changes are complex and diverse. Only from the perspective of land use types cannot fully explain the changes in ET, and the influence of climate factors is also an important factor.

Generally speaking, climate factors are prerequisite for surface energy supply, determining the maximum actual surface evapotranspiration. However, in arid and semi-arid environments, vegetation canopy serves as interceptor of energy flux and hence determines the range of surface evapotranspiration[52]. As the main vegetation and land use type in the Yinchuan Plain, cropland accounts for about 60% of the total area. In Figure 1, the vegetation cover of the Yinchuan Plain during the growing season (June to August) is shown. Comparing Figure 6, it can be seen that in the time series studied, the evapotranspiration changed only significantly in a small number of areas, such as bare land conversions into farmlands, wetlands, or water bodies. Most areas did not show significant changes in evapotranspiration within the study period, such as farmland. This is consistent with the findings of Xiaomei Jin et al. in their study of the Yinchuan Plain from 2001 to 2014. This indicates that the trend of ET changes in the Yinchuan Plain area is mainly dominated by changes in cropland and land cover types, with meteorological factors as secondary influences. Through studying the changes in ET_a, it is possible to better understand the water consumption by vegetation and land and adjust the allocation agricultural water resources in a timely manner (such as irrigation), and improve the efficiency of freshwater resource utilization (avoiding inefficient water use or irrigation water shortage). Meanwhile, the attribution analysis of surface evapotranspiration changes in the Yinchuan Plain will be the focus of subsequent research, which has guiding significance for clarifying the direction of water resource management and sustainable development in the region.

4.2. The Uncertainty Analysis of geeSEBAL

Because of the impact of observational conditions, the validation data gathered from weather stations was not continuous, and there were missing measurements in some study dates and years. Therefore, the large evapotranspiration values from four stations with a relatively complete dataset and the small evapotranspiration values from six stations were selected for validation. Based on our findings the estimation results of the geeSEBAL were within reasonable margin of errors. Even if there were some stations with weak correlations, it would have been due to the closure mode of the surface energy[36]. According to Laipelt[36], the main challenge faced by the geeSEBAL program is the selection of end members and the definition of a spatial scope. The geeSEBAL model is highly sensitive to the spatial scope, and the calibration function of cold and hot end members can significantly improve the accuracy of ET estimation[53]. This study upgraded the estimation method of ET from single image to batch estimation in order to achieve high consistency in ET inversion over spatial range and time span (Figure 10.). Therefore, the same calibration end members were set for multiple images on the same date. This affected the estimation accuracy in some areas to some extent, but the overall ET estimation showed satisfactory results (Figure 2.). It can also be seen that the geeSEBAL has a great potential for estimating ET over small areas, and adjusting the calibration end members based on actual situation to achieve a higher estimation accuracy.

Due to the scarcity of high-quality remote sensing images in Google Earth Engine and the lack of observation data from meteorological stations, it was difficult to extrapolate ET to both monthly and annual time scales. Therefore, the ET trend analysis for long time series only considered the estimated ET representing dates as an example. By the same token, we conducted no further analysis of the sensitivity and contribution of meteorological factors to the ET. This can be used as an additional extension in future research to fully comprehend the pattern of changes in evapotranspiration in the Yinchuan Plain.

 doi:10.20944/preprints202408.0555.v1

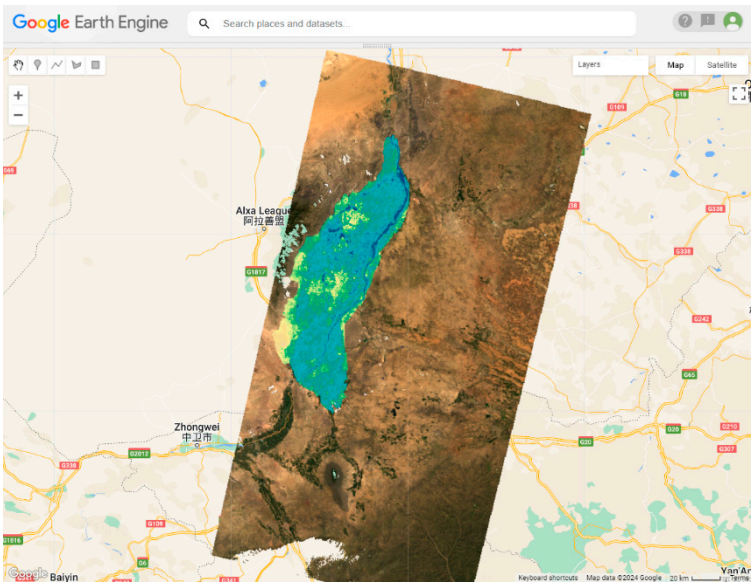

Figure 10. The geeSEBAL with batch image estimation mode.

Unlike previous studies on ET in the Yinchuan Plain by Wang Zhuoyue et al[54], the GEE online dataset in this study can used to quickly obtain continuous high spatiotemporal resolution ET values around the world. While the accuracy of meteorological datasets can impact the geeSEBAL model, this problem can be mitigated by using the automatic calibration option of endpoints or by restricting the study area. This ensures that the ET distribution maps generated fulfill the necessary criteria. The ET values for different land use types can also be quickly calculated based on the CLCD, avoiding the cumbersome image processing in the traditional remote sensing techniques to estimate evapotranspiration. This greatly reduces the inversion time for regional evapotranspiration, and fully leverages the advantages of remote sensing technology in regional water resource management.

5. Conclusions

This study was conducted in the Yinchuan Plain, the irrigation area of the Yellow River Basin. The open-source SEBAL framework was used to verify the applicability of the model in the Yinchuan Plain through the Application Programming Interface (API) to estimate ET and to evaluate its distribution pattern across different underlying surfaces.

In spring, the daily ET of the Yinchuan Plain was found to be mainly concentrated in the central lake wetland area, with a maximum value of 4.32 mm day^{-1}. In summer, the daily ET was found to be concentrated in the cultivated land and water areas, with a maximum value of 6.90 mm day^{-1}. The ET values were highest in Autumn and winter new the water bodies and impervious areas, with maximum values of 3.93 mm day^{-1} and 1.56 mm day^{-1}, respectively.

From 1987 to 2020, the ET of the Yinchuan Plain showed an obvious upward and downward trend in some areas with significant land use changes, but the overall ET of the region remained relatively stable without dramatic fluctuations.

The evapotranspiration of different underlying land use types in the Yinchuan Plain region is as follows: water body>cultivated land>impervious areas>grassland>bare land. The evapotranspiration of water bodies ranges from 5.03 to 7.62 mm day^{-1}, cropland from 4.16 to 6.36 mm day^{-1}, impervious areas from 3.28 to 5.27 mm day^{-1}, grasslands from 2.07 to 3.78 mm day^{-1}, and bare land from 0.81 to 2.67 mm day^{-1}. The study shows that the distribution pattern of regional evapotranspiration is not only influenced by climate conditions, but it is also closely related to human activities.

Author Contributions: For research articles with several authors, the following statements should be used "Conceptualization, X.X. and Y.Y.; methodology, X.X.; software, X.X.; validation, X.X., Y.Y. and Z.Z.; formal analysis, X.X.; investigation, X.X.; resources, X.X.; data curation, X.X.; writing—original draft preparation, X.X.;

writing—review and editing, X.X.; visualization, X.X.; supervision, X.X.; project administration, X.X.; funding acquisition, Y.Y. All authors have read and agreed to the published version of the manuscript."

Funding: This research was funded by the National Natural Science Foundation of China (Grant number 41901285 and 41972261) and Training Plan for Young Backbone Teachers in Higher Education Institutions in Henan Province(Grant number 2023GGJS073).

Data Availability Statement: The data are available from the corresponding author upon reasonable requests.

Conflicts of Interest: The authors declare no conflicts of interest.

References

1. Priestley, C.H.B.; Taylor, R.H. On the assessment of surface heat flux and evaporation using large-scale parameters[J]. *Mon. Weather Rev.* **1972**, 100, 81-92.
2. Resenberg, N.J.; Blad, B.L.; Verma, S.B. Microclimate: The biological environment of plants[J]. **1983**.
3. Chen, H.; Yang, D.W.; Lv, H.F. Comparison of temporal extrapolation methods for evapotranspiration over variant underlying croplands[J]. *Transactions of the Chinese Society of Agricultural Engineering*. **2013**, 29, 73-81.
4. Brown, K.W.; Rosenberg, N.J. A resistance model to predict evapotranspiration and its application to a sugar beet field 1[J]. *Agron. J.* **1973**, 65, 341-7.
5. Paniconi, C.; Putti, M. Physically based modeling in catchment hydrology at 50 Survey and outlook[J]. *Water Resour. Res.* **2015**, 51, 7090-129.
6. Gao, Y.C.; Long, D. Progress in Models for Evapotranspiration Estimation Using Remotely Sensed Data[J]. *National Remote Sensing Bulletin*. **2008**, 515-28.
7. Li, X.Y.; Yu, D.Y. Progress on Evapotranspiration Estimation Methods and Driving Forces in Arid and Semiarid Regions[J]. *Arid Zone Research*. **2020**, 37, 26-36.
8. Zhang, R.H.; Sun, X.M.; Liu, J.Y. Regional variations in crop transpiration and soil water utilization by quantitative remote sensing inversion[J]. *Scientia Sinica(Terrae)*. **2001**, 959-68.
9. Zhao, T.W.; Zhu, W.B.; Pei, L. Remote Sensing Estimation of Terrestrial Evapotranspiration and Analysis of Its Temporal-spatial Distribution Characteristics over the Three-River Headwater Region[J]. *Remote Sensing Technology and Application*. **2022**, 37, 137-47.
10. Carlson, T.N.; Capehart, W.J.; Gillies, R.R. A new look at the simplified method for remote sensing of daily evapotranspiration[J]. *Remote Sens. Environ.* **1995**, 54, 161-7.
11. Seguin, B.; ITIER, B. Using midday surface temperature to estimate daily evaporation from satellite thermal IR data[J]. *Int. J. Remote Sens.* **1983**, 4, 371-83.
12. Zhang, R.H.; Sun, X.M.; Zhu, Z.L. Differential thermal inertia-based full remote sensing information model of surface evaporation and its validation in Shapotou area, Gansu, China[J]. *Scientia Sinica(Terrae)*. **2002**, 1041-50.
13. Engman, E.T. Recent advances in remote sensing in hydrology[J]. *Rev. Geophys.* **1995**, 33, 967-75.
14. Menenti, M.; Choudhury, B.J. Parameterization of land surface evaporation by means of location dependent potential evaporation and surface temperature range[J]. **1993**.
15. Bastiaanssen, W.G.M.; Menenti, M.; Feddes, R.A. A remote sensing surface energy balance algorithm for land (SEBAL). 1. Formulation[J]. *J. Hydrol.* **1998**, 212, 198-212.
16. Bastiaanssen, W.G.M.; Pelgrum, H.; Wang, J.; Al, E. A remote sensing surface energy balance algorithm for land (SEBAL). Part 2 Validation[J]. *J. Hydrol.* **1998**, 212, 213-29.
17. Jin, K.L.; Hao, L. Evapotranspiration estimation in the Jiangsu-Zhejiang-Shanghai Area based on remote sensing data and SEBAL model[J]. *Remote Sensing for Natural Resources*. **2020**, 32, 204-12.
18. Gong, Z.N.; Lu, L.; Jin, D.D.; Ackermann, K. Remote sensing estimation of evapotranspiration and ecological water demand in Zhalong wetland under land use/cover change[J]. *Acta Ecologica Sinica*. **2021**, 41, 3572-87.
19. Li, X.L.; Yang, L.X.; Xue, X.X. Analysis of evapotranspiration pattern by SEBAL model during the growing season in the agro-pastoral ecotone in Northwest China[J]. *Acta Ecologica Sinica*. **2020**, 40, 2175-85.
20. Su, Z.; Schmugge, T.; Kustas, W.P. An Evaluation of Two Models for Estimation of the Roughness Height for Heat Transfer between the Land Surface and the Atmosphere[J]. *J. Appl. Meteorol. Climatol.* **2001**, 40, 1933-51.
21. Zhang, D.; Wei, Z.; Feng. Analysis of evapotranspiration estimation and its spatial-temporal characteristics: taking Zhanghe irrigation district as an example[J]. *Bulletin of Surveying and Mapping*. **2022**, 57-63.
22. Su, Z. The Surface Energy Balance System (SEBS) for estimation of turbulent heat fluxes[J]. *Hydrol. Earth Syst. Sci.* **2002**, 6, 85-100.
23. Senay, G.B.; Bohms, S.; Singh, R.K. Operational Evapotranspiration Mapping Using Remote Sensing and Weather Datasets A New Parameterization for the SSEB Approach[J]. *Jawra Journal of the American Water Resources Association*. **2013**, 49, 577-91.

24. Bhattarai, N.; Shaw, S.B.; Quackenbush, L.J. Evaluating five remote sensing based single-source surface energy balance models for estimating daily evapotranspiration in a humid subtropical climate[J]. *Int. J. Appl. Earth Obs. Geoinf.* **2016**, 49, 75-86.
25. Tasumi, M.; Trezza, R.; Allen, R.G.; Al, E. Operational aspects of satellite-based energy balance models for irrigated crops in the semi-arid US[J]. *Irrigation and Drainage Systems*. **2005**, 19, 355-79.
26. Allen, R.; Irmak, A.; Trezza, R.; Al, E. Satellite-based ET estimation in agriculture using SEBAL and METRIC[J]. *Hydrol. Process.* **2011**, 25, 4011-27.
27. Laipelt, L.; Ruhoff, A.L.; Fleischmann, A.S. Assessment of an automated calibration of the SEBAL algorithm to estimate dry-season surface-energy partitioning in a forest–savanna transition in Brazil[J]. *Remote Sens.* **2020**, 12, 1108.
28. Long, D.; Singh, V.P.; Li, Z.L. How sensitive is SEBAL to changes in input variables, domain size and satellite sensor?[J]. *Journal of Geophysical Research*. **2011**, 116.
29. Shuttleworth, W.J.; Gurney, R.J.; Hsu, A.Y. FIFE The variation in energy partition at surface flux sites[J]. *Iahs Publ*. **1989**, 186, 523-34.
30. Shuttleworth, W.J. Macrohydrology—The new challenge for process hydrology[J]. *J. Hydrol.* **1988**, 100, 31-56.
31. Shuttleworth, W.J.; Gurney, R.J. The theoretical relationship between foliage temperature and canopy resistance in sparse crops[J]. *Q. J. R. Meteorol. Soc.* **1990**, 116, 497-519.
32. Ke, Y.; Im, J.; Park, S.; Al, E. Downscaling of MODIS one kilometer evapotranspiration using Landsat-8 data and machine learning approaches[J]. *Remote Sens.* **2016**, 8, 215.
33. Muñoz-Sabater, J.; Dutra, E.; Agustí-Panareda, A.; Al, E. ERA5-Land: A state-of-the-art global reanalysis dataset for land applications[J]. *Earth Syst. Sci. Data*. **2021**, 13, 4349-83.
34. Hersbach, H.; Bell, B.; Berrisford, P.; Al, E. The ERA5 global reanalysis[J]. *Q. J. R. Meteorol. Soc.* **2020**, 146, 1999-2049.
35. Shuttleworth, W.J. Terrestrial hydrometeorology[M]. *John Wiley & Sons*. **2012**.
36. Laipelt, L.; Kayser, R.H.B.; Fleischmann, A.S. Long-term monitoring of evapotranspiration using the SEBAL algorithm and Google Earth Engine cloud computing[J]. *Isprs Journal of Photogrammetry and Remote Sensing*. **2021**, 178, 81-96.
37. Allen, R.G.; Pereira, L.S.; Raes, D.; Al, E. FAO Irrigation and drainage paper No. 56[J]. *Rome: Food and Agriculture Organization of the United Nations*. **1998**, 56, e156.
38. REN, G.G.J. Change in pan evaporation and the influential factors over China 1956-2000[J]. *Journal of Natural Resources*. **2006**, 21, 31-44.
39. GB/T 35230-2017. Specification for Surface Meteorological Observations - Evaporation[S]. *In China Meteorological Administration*. **2017**.
40. Yang, J.; Huang, X. 30 m annual land cover and its dynamics in China from 1990 to 2019[J]. *Earth System Science Data Discussions*. **2021**, 2021, 1-29.
41. Tasumi, M.; Allen, R.G.; Trezza, R. At-surface reflectance and albedo from satellite for operational calculation of land surface energy balance[J]. *J. Hydrol. Eng.* **2008**, 13, 51-63.
42. IFS Documentation CY41R2. IFS Documentation CY41R2 - Part VII: ECMWF Wave Model[S]. *European Centre for Medium-Range Weather Forecasts*. **2016**.
43. Buck, A.L. New equations for computing vapor pressure and enhancement factor[J]. *Journal of Applied Meteorology (1962-1982)*. **1981**, 1527-32.
44. Alduchov, O.A.; Eskridge, R.E. Improved Magnus form approximation of saturation vapor pressure[J]. *J. Appl. Meteorol. Climatol.* **1996**, 35, 601-9.
45. Allen, R.G.; Burnett, B.; Kramber, W.; Al, E. Automated calibration of the metric-landsat evapotranspiration process[J]. *Jawra Journal of the American Water Resources Association*. **2013**, 49, 563-76.
46. Sung, J.H.; Chung, E.S.; Kim, Y.; Al, E. Meteorological hazard assessment based on trends and abrupt changes in rainfall characteristics on the Korean peninsula[J]. *Theor. Appl. Climatol.* **2017**, 127, 305-26.
47. Hao, X.; Chen, Y.; Xu, C. Impacts of climate change and human activities on the surface runoff in the Tarim River Basin over the last fifty years[J]. *Water Resour. Manag.* **2008**, 22, 1159-71.
48. Jin, X.; Zhu, X.; Xue, Y. Satellite-based analysis of regional evapotranspiration trends in a semi-arid area[J]. *Int. J. Remote Sens.* **2019**, 40, 3267-88.
49. Yang, L.; Feng, Q.; Zhu, M.; Wang, L.; Alizadeh, M.R.; Adamowski, J.F.; Wen, X.; Yin, Z. Variation in actual evapotranspiration and its ties to climate change and vegetation dynamics in northwest China[J]. *Journal of Hydrology (Amsterdam)*. **2022**, 607, 127533.
50. Ning, T.; Li, Z.; Feng, Q.; Li, Z.; Qin, Y. Attribution of growing season evapotranspiration variability considering snowmelt and vegetation changes in the arid alpine basins[J]. *Hydrol. Earth Syst. Sci.* **2021**, 25, 3455-69.
51. Wang, Y.; Liu, B.; Su, B.; Zhai, J.; Gemmer, M. Trends of Calculated and Simulated Actual Evaporation in the Yangtze River Basin[J]. *J. Clim.* **2011**, 24, 4494-507.

 doi:10.20944/preprints202408.0555.v1

52. Qiu, G.Y. Water and energy: evapotranspiration, thermal environment, and energy balance[M]: Science Press, 2014.
53. Tang, R.; Li, Z. L.; Chen, K. S.; et al. Spatial-scale effect on the SEBAL model for evapotranspiration estimation using remote sensing data[J]. Agricultural and forest meteorology, 2013, 174.
54. Wang, Z.Y.; Kong, J.L.; Li, Y.; Zhang, Z.Y.; Liu, H.H.; Jiang, Y.Z.; Zhong, Y.L.; Zhang, J.Y. An analysis of spatio-temporal characteristics and influencing factors of surface evapotranspiration in the Yinchuan Plain based on MOD16 data[J]. *Hydrogeology and Engineering Geology*. **2021**, 48, 53-61.